Geophysical Journal International

Geophys. J. Int. (2019) **216,** 123–129
Advance Access publication 2018 October 09
GJI Geomagnetism, rock magnetism and palaeomagnetism

doi: 10.1093/gji/ggy416

EXPRESS LETTER

Torsional waves driven by convection and jets in Earth's liquid core

R.J. Teed,[1] C.A. Jones[2] and S.M. Tobias[2]

[1]*School of Mathematics and Statistics, University of Glasgow, Glasgow G12 8QQ, UK. E-mail: Robert.Teed@glasgow.ac.uk*
[2]*Department of Applied Mathematics, University of Leeds, Leeds LS2 9JT, UK*

Accepted 2018 October 8. Received 2018 October 3; in original form 2018 April 24

SUMMARY

Turbulence and waves in Earth's iron-rich liquid outer core are believed to be responsible for the generation of the geomagnetic field via dynamo action. When waves break upon the mantle they cause a shift in the rotation rate of Earth's solid exterior and contribute to variations in the length-of-day on a ∼6-yr timescale. Though the outer core cannot be probed by direct observation, such torsional waves are believed to propagate along Earth's radial magnetic field, but as yet no self-consistent mechanism for their generation has been determined. Here we provide evidence of a realistic physical excitation mechanism for torsional waves observed in numerical simulations. We find that inefficient convection above and below the solid inner core traps buoyant fluid forming a density gradient between pole and equator, similar to that observed in Earth's atmosphere. Consequently, a shearing jet stream—a 'thermal wind'—is formed near the inner core; evidence of such a jet has recently been found. Owing to the sharp density gradient and influence of magnetic field, convection at this location is able to operate with the turnover frequency required to generate waves. Amplified by the jet it then triggers a train of oscillations. Our results demonstrate a plausible mechanism for generating torsional waves under Earth-like conditions and thus further cement their importance for Earth's core dynamics.

Key words: Core; Dynamo: theories and simulations; Magnetic field variations through time; Numerical modelling.

1 INTRODUCTION

The geomagnetic field is generated deep inside the Earth in the region known as the fluid outer core (Roberts & King 2013). Chaotic motions of the iron-rich fluid driven primarily by thermal and compositional convection (Jones 2015) continuously replenish the geomagnetic field via dynamo action (Jones 2011). Records of secular variation (Bloxham & Gubbins 1985; Jackson *et al.* 2000) demonstrate that the field varies across a range of timescales. Most well known are the reversals of the field, occurring on average every 200 000 yr over the last 15 million years (McElhinny & McFadden 1998). However, features also exist that operate on much shorter timescales (Jackson 1997; Bloxham *et al.* 2002) with recent observational evidence (Buffett *et al.* 2009; Gillet *et al.* 2010, 2015) appearing to show variations including the ∼6-yr signal observed in the change of length-of-day (Holme & de Viron 2013). It has been widely suggested that this signal arises owing to torsional waves (TWs; Taylor 1963; Braginsky 1970; Zatman & Bloxham 1997; Buffett *et al.* 2009; Gillet *et al.* 2010; Wicht & Christensen 2010; Teed *et al.* 2014, 2015) operating inside the core propagating from the 'tangent cylinder' (TC, the theoretical cylinder aligned with the rotation axis that circumscribes the solid inner core—see Fig. 1) and the coupling of the fluid and solid parts of Earth's interior at the core–mantle boundary (CMB). The speed of TWs can also be used to infer information about the magnetic field strength in the core where direct geomagnetic observations are not possible (Gubbins & Bloxham 1985). Recent observations from the European Space Agency's Swarm satellite mission have revealed changes in the high latitude field. These data have contributed, along with analysis of previous data, to the inferral of a strong fluid jet on the TC (Livermore *et al.* 2017). This jet was found to be accelerating; its speed was only 15–20 km yr^{-1} up until 2004 but by 2017 had reached 40 km yr^{-1}. This is consistent with an azimuthal flow in our simulations that exists at the location where TWs are driven. The time-varying jets (discussed later) can be either westwards or eastwards and reach a similar magnitude to those observed by Livermore *et al.* (2017).

2 NUMERICAL EXPERIMENTS AND THEORY

Owing to the lack of direct measurement of magnetic features below the CMB, numerical experiments and theory are essential tools

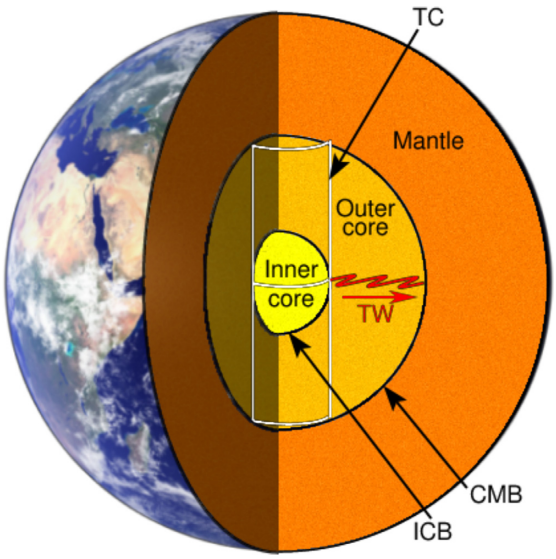

Figure 1. Schematic of torsional waves in the core. A cutaway diagram showing the layers of Earth from the crust to the inner core. Solid white lines show the location of the imaginary 'tangent cylinder' (TC), running vertically from pole-to-pole in the outer core and circumscribing the inner core. The red line indicates the possible trajectory of a torsional wave (TW) in the outer core from the inner core boundary (ICB) to the core–mantle boundary (CMB). The transverse torsional wave propagates radially from the TC to the CMB with its oscillations in the azimuthal direction.

(Christensen & Wicht 2015). TWs are manifestations of the violation of the leading order 'magnetostrophic' balance in the outer core (Taylor 1963); this loss of balance leads to the longitudinal acceleration of concentric cylinders of fluid, with the wave itself propagating (cylindrically) radially (Braginsky 1970). TWs have now been isolated in several sets of fully 3-D spherical dynamo simulations (Wicht & Christensen 2010; Teed *et al.* 2014, 2015; Schaeffer *et al.* 2017). In particular, a recent simulation has displayed TWs originating at the TC in a periodic fashion on timescales similar to Earth's ∼6-yr signal (Teed *et al.* 2015). However, despite this progress, a critical question hitherto remains unanswered: how are these waves actually *excited* in the core? We address this by performing high-resolution numerical simulations of magnetoconvection operating within a spherical shell. Emphasis is placed on the region at the TC where periodic waves primarily originate, and where a jet is formed.

We solve a standard set of equations governing the time evolution of velocity, magnetic induction and temperature subject to solenoidal conditions for the velocity and magnetic field. We use a spherical coordinate system (r, θ, ϕ) and consider a fluid-filled spherical shell of aspect ratio $r_i/r_o = 0.35$, where r_i and r_o are the radial positions of the inner and outer boundaries. Gravity acts radially inwards ($\mathbf{g} = -g\hat{\mathbf{r}}$) and the shell rotates with rotation rate $\Omega = \Omega\hat{\mathbf{z}}$, where z is the vertical direction in cylindrical polar coordinates. The fluid itself is modelled using the Boussinesq approximation (i.e. an incompressible fluid) and has constant values of density ρ, thermal expansivity α, kinematic viscosity ν, thermal diffusivity κ, and magnetic diffusivity, η. A temperature gradient to provide thermal convection is enabled by setting temperature, $T = \Delta T$ at $r = r_i$ and $T = 0$ at $r = r_o$. Kinematic/thermal boundary conditions are no-slip/fixed temperature at both boundaries. For the implementation of magnetoconvection a persistent magnetic field must be imposed. This is achieved by setting the amplitude of the axial dipole component (spherical harmonic, Y_{10}) such that $\mathbf{B_0} = (2B_0\cos\theta, B_0\sin\theta, 0)$ at $r = r_o$. On all remaining components of the field, both at $r = r_o$ and at $r = r_i$, the standard form of insulating magnetic boundary conditions is applied.

The equations for momentum, temperature and magnetic induction are non-dimensionalized using length scale $D = r_o - r_i$, magnetic timescale D^2/η, magnetic scale $\sqrt{\rho\mu_0\Omega\eta}$ and temperature scale, ΔT. This introduces several non-dimensional parameters into the equations: the Ekman number, $E = \nu/\Omega D^2$, Rayleigh number, $Ra = g\alpha\Delta T D^3/\nu\kappa$, Prandtl number, $Pr = \nu/\kappa$, and magnetic Prandtl number, $Pm = \nu/\eta$. The resulting non-dimensional equations for the velocity, $\mathbf{u}$, magnetic field, $\mathbf{B}$ and temperature, T are

$$\frac{\partial \mathbf{u}}{\partial t} + (\mathbf{u}\cdot\nabla)\mathbf{u} = -\frac{Pm}{E}\left[\nabla p + 2\hat{\mathbf{z}}\times\mathbf{u} - (\nabla\times\mathbf{B})\times\mathbf{B}\right] + \frac{Pm^2 Ra}{Pr} T\mathbf{r} + Pm\nabla^2\mathbf{u}, \tag{1}$$

$$\frac{\partial T}{\partial t} + (\mathbf{u}\cdot\nabla)T = \frac{Pm}{Pr}\nabla^2 T, \tag{2}$$

$$\frac{\partial \mathbf{B}}{\partial t} - \nabla\times(\mathbf{u}\times\mathbf{B}) = \nabla^2\mathbf{B}, \tag{3}$$

$$\nabla\cdot\mathbf{u} = 0, \tag{4}$$

$$\nabla\cdot\mathbf{B} = 0. \tag{5}$$

For the primary simulation discussed here (further simulations are discussed in the Supporting Information) the non-dimensional parameters take the values: $E = 5\times10^{-6}$, $Ra = 1.8\times10^{8}$, $Pr = 1$, Pm

Table 1. Definitions of quantities. Overbars and angle brackets represent averages over ϕ and z, respectively.

Quantity	Description	Definition
$\tilde{\mathbf{u}}$	Mean velocity	$\tilde{\mathbf{u}}(s,\phi,z)=\frac{1}{\tau}\int_0^\tau \mathbf{u}\,dt$
$\mathbf{u}'$	Fluctuating velocity	$\mathbf{u}'(t,s,\phi,z)=\mathbf{u}-\tilde{\mathbf{u}}$
u'_g	Geostrophic speed	$u'_g(t,s)=\langle\overline{u'_\phi}\rangle$
$\mathbf{u}'_\mathbf{a}$	Ageostrophic velocity	$\mathbf{u}'_\mathbf{a}(t,s,\phi,z)=\mathbf{u}'-u'_g\hat{\boldsymbol{\phi}}$
$u'_{a\phi}$	Ageostrophic azimuthal speed	$u'_{a\phi}(t,s,\phi,z)=\hat{\boldsymbol{\phi}}\cdot\mathbf{u}'_\mathbf{a}$
U_A	Alfvén speed	$U_A(s)=\sqrt{\frac{Pm}{E}\langle\overline{B_s^2}\rangle}$

$=0.1$ as well as imposed field strength $B_0=10$. For comparison the current expected values in Earth's outer core are: $E\sim10^{-15}$, $Ra\sim10^{30}$, $Pr\sim0.1$, $Pm\sim10^{-6}$. Conversion between non-dimensional time and physical time (in years) is achieved by equating the Alfvén speed from our simulation at $r=r_o$ to Earth's observed value at the CMB ($U_A^E\sim1.8\times10^{-3}$ ms^{-1}, calculated from the radial magnetic field). This matching of speeds gives a timescale such that one unit of non-dimensional time in our primary simulation (simulation 1) is equivalent to ∼700 yr of real time. The code used to perform simulations is the 'Leeds spherical dynamo code' (Willis *et al.* 2007). It has been developed over a number of years and has been successfully benchmarked against other international codes to ensure accuracy (Christensen *et al.* 2001; Jones *et al.* 2011).

For diagnostics of TWs we also convert to cylindrical geometry, (s,ϕ,z), where rotation is aligned with the z-axis. A short segment (∼35 yr in duration) of our primary simulation is inspected where TWs are known to be present (Teed *et al.* 2015). Timescales over this interval are separated so that for any quantity, A, we have $A=\tilde{A}+A'$ where $\tilde{A}$ is the mean (time averaged) part of A and A' is the fluctuating component.

Of the three potential sources of forcing—Reynolds, Lorentz and viscous—of TWs hitherto proposed (Wicht & Christensen 2010), the Lorentz force has been shown to be the principal driver of TWs as the parameters approach more Earth-like values (Teed *et al.* 2015; Schaeffer *et al.* 2017). However, to determine the excitation mechanism of TWs we have identified which of the many terms that make up the Lorentz force (see the Supporting Information) are largest in magnitude. Crucially, we find that terms coupling the mean magnetic field to the convective ageostrophic speed, $u'_{a\phi}$, account for approximately 87 per cent of the total Lorentz force; here $u_\phi=\tilde{u}_\phi+u'_g+u'_{a\phi}$ so that the fluctuating part of u_ϕ is split into a geostrophic part, u'_g (representing the TW) and an ageostrophic part, $u'_{a\phi}$ (representing convection). Table 1 gives a summary of the definitions involved.

3 AN EXCITATION MECHANISM FOR TORSIONAL WAVES

The clear periodic form of the TW signal in Fig. 2 is very reminiscent of the equivalent plot for the core-flow model data (Gillet *et al.* 2010, 2015). The strong excitation of waves at the TC, coupled with the importance of $u'_{a\phi}$ in the Lorentz force, suggests that the frequency of the convection is matching to the frequency of the TWs themselves. Indeed, waves are excited from the TC on a period that corresponds to ∼6 yr with reasonable estimates of the field strength at the CMB. Fig. 3(a) shows the ageostrophic velocity, the total angular velocity, $\omega'=|(\mathbf{r}\times\mathbf{u}')/r^2|$, and the vertical parts of the velocity and vorticity, ζ'_z, all fluctuating on the same ∼6-yr timescale. In particular, the axisymmetric ageostrophic convection (shown by the red curve) is almost in phase with the TW signal but precedes it slightly indicating its role in wave excitation. Furthermore, Fig. 3(b) shows the match in frequency (calculated as the spectrum from the data points of the time-series) between the power spectra of the TW and the modes of ageostrophic convection. However, a TW requires an *axisymmetric* excitation mechanism, so how does the *non-axisymmetric* ageostrophic convection provide this? Figs 4(a)–(c) show the structure of convection in a horizontal slice at depth 1700 km above the equatorial plane. When the TW (Fig. 4b) is subtracted from the overall velocity seen in Fig. 4(a), clear convective cells appear throughout the core. In particular, on the TC itself there exist small patches of convection in the form of approximately 20 cyclones and anticyclones (Fig. 4c). These modes of convection are excited by a region of sharp temperature gradient found at the TC. The thinness of this layer determines the size of the convection, and the small size of these eddies (∼150 km in diameter) is an essential ingredient for exciting TWs; smaller convective modes have *shorter* turnover times operating on the same timescale as the TW. Although the convection here is clearly non-axisymmetric, it does contain an axisymmetric component created through the nonlinear interaction of modes. Therefore a picture emerges whereby the axisymmetric part of the convection is able to resonate with the TW owing to the contribution of the small-scale modes of convection. The frequency of the TW itself is set by the resonant cavity inside the TC as waves travel from the TC to the polar axis and back (see Supporting Information Video S1).

By considering the power spectrum of the ageostrophic convection (Fig. 3b) we are able to validate the theory described above. Power is concentrated around a period of ∼6.25 yr (equivalent to a frequency of ∼0.16 yr^{-1} as seen in the plot) and azimuthal wavenumbers, $m=0$ (axisymmetric) and $17\le m\le24$ (corresponding to the ∼20 patches of convection seen in Fig. 4). Thus these localized patches of convection, despite their individual random frequencies and phases, sum to deliver an axisymmetric component operating with the same frequency allowing the excitation of TWs.

The thermal gradient across the TC (Supporting Information Fig. S1) described above also leads to the formation of a strong jet evidenced by a strong negative (westward) velocity and shear layer near the TC in Fig. 4(d). Jets are transient, yet persistent, features located at the TC that come and go on a timescale longer than that of the TWs. The jets can thus be more clearly identified in plots which display a snapshot at a specific time (Supporting Information Fig. S2), rather than the time-averaged data shown in Fig. 4(d). In our simulation the jet has a characteristic velocity of ∼50 km yr^{-1}, which is comparable with the observations (Livermore *et al.* 2017). The mean radial magnetic field at the TC is also shown; this is vital both to control the size of the eddies and to contribute to the Lorentz force driving the waves. If the radial field near the TC is too small, convective cells at small E are very small-scale (Jones 2015); if the radial field near the TC is significantly larger, our simulations show larger scale convective vortices which have too long a period to resonate with the TW frequency. Moreover, convection at the TC persists throughout the depth of the core, evidenced by the eddies seen in the vorticity plots of Figs 4(e)–(g). Also apparent in these plots is the inefficiency of convection inside the TC (Sreenivasan & Jones 2006). Buoyant material is trapped there, leading to the temperature gradient and resulting jet stream. The time evolution of vorticity in Figs 4(e)–(g) also highlights the resonant cavity effect acting on the TWs. Axisymmetric vorticity seen at $t=13$ yr (Fig. 4e) vanishes at $t=14.5$ yr (Fig. 4f) and is replaced by axisymmetric vorticity of opposite sign by $t=16$ yr (Fig. 4g). This represents the

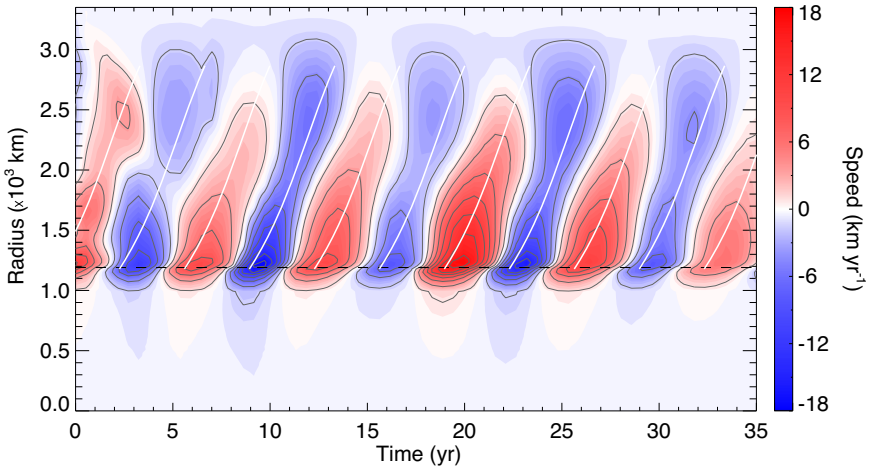

Figure 2. Torsional wave signal. Colour density plot of the azimuthal fluctuating velocity, u'_ϕ, averaged over depth, z, and azimuth, ϕ. The repeating blue and red pattern shows a train of waves propagating in time in the radial direction. Waves clearly originate at the TC (indicated in s-space by the horizontal black dashed line) and travel in the region of the core outside the TC ($s > 1200$ km) towards the mantle at $s = 3400$ km. The point of excitation is just inside the TC where $1000\,\text{km} < s < 1200\,\text{km}$. White curves indicate the trajectory expected of a wave travelling at the Alfvén speed (calculated from the magnetic field, **B**) and are overlaid on the train of waves in order to emphasize the excellent match.

TWs travelling from the TC to the polar axis and back; this sets the TW frequency.

4 DISCUSSION AND CONCLUSIONS

We note that the periodic train of waves observed has been produced using a magnetoconvection rather than a dynamo model. This allows parameter regimes closer to that of Earth's core to be reached; in particular, regimes with a larger magnetic field and smaller viscosity. Previous dynamo studies (Sreenivasan & Jones 2006), which are not in this regime, cannot produce such a strong temperature gradient at the TC interacting with strong magnetic fields; in those models the convection does not occur with such large wavenumbers. Previous studies on TWs (Wicht & Christensen 2010; Teed *et al.* 2014) do not display clear periodic waves for the same reason. To ensure the robustness of our result we have performed several simulations in nearby parameter space (Supporting Information Figs S3–S5), which give broadly similar results. As the input parameters of the simulation are varied we find that the frequencies of the convection and TWs vary (Supporting Information Fig. S4). This can lead to the intermittent, or quasi-periodic, excitation of waves where there are significant intervals with weak TWs (Supporting Information Fig. S5). Indeed, periodic patterns of TWs vanish altogether if the values of the frequencies differ significantly.

Another recent model (Gillet *et al.* 2017) has argued that the resonant cavity that determines the ∼6-yr period exists in the outer core, rather than within the TC. However, neither recent low viscosity dynamo simulations (Schaeffer *et al.* 2017) nor our simulations show evidence of the reflection of waves at the CMB that is required for that scenario to work. In fact, fig. 21 of Schaeffer *et al.* (2017) has similarities with our convection model, with torsional waves emerging from the TC. Note also that their model has more convection inside the TC than ours, but this does not apparently impede the generation of TWs near the TC. It may be that reflection would become more apparent with even lower viscosity, but it could also be that the mismatch of the spherical CMB boundary with the cylindrical propagation of torsional waves prevents the outer core from being an effective resonant cavity. If a conducting layer at the base of the mantle is included, an outer core resonant cavity might be possible, but then such a layer is likely to damp any TWs strongly (Roberts & Aurnou 2012). Our focus has been on the excitation mechanism found in simulations that exhibit the crucial properties of TWs as identified in *observations*: periodic excitation at the TC and an intradecadal operational timescale.

The extremely small viscosity in Earth's core means that it is not computationally possible to resolve the small scales of convection that must exist. This is typical of all simulations that model core dynamics. Analysis of several other simulations from our full suite shows that TWs often do not operate in such an Earth-like periodic manner (Teed *et al.* 2015). However, we believe that this

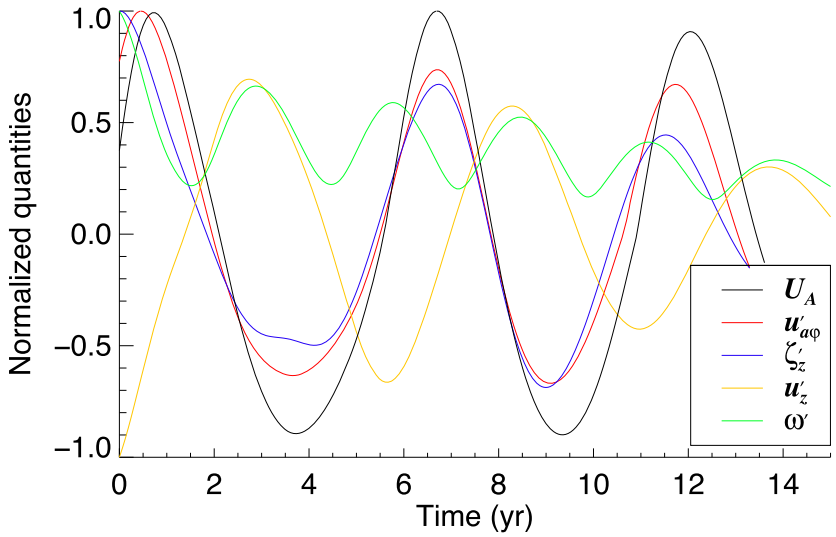

(a)

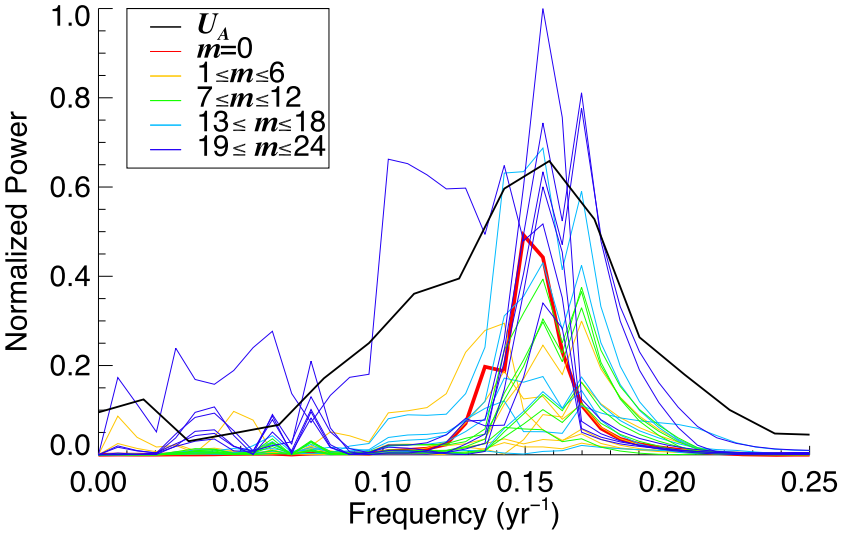

(b)

Figure 3. Torsional wave and convective periodicity. (a) Time-series plot of quantities at $s = r_i$ and $z = r_i$ (on the TC). All quantities are averaged in azimuth, ϕ, and normalized using their maximum absolute value [max $(|U_A|) = 12.3$ km yr^{-1}, max$(|u'_{a\phi}|) = 3.5$ km yr^{-1}, max$(|\zeta'_z|) = 0.09$ yr^{-1}, max$(|u'_z|) = 1.7$ km yr^{-1}, max $(|\omega'|) = 0.02$ yr^{-1}]. Each coloured line shows a different quantity given in the key. (b) Power spectrum of the ageostrophic convective velocity calculated at $s = r_i$ and $z = r_i$ and normalized by the largest spectral mode. Coloured lines show profiles that are grouped for values of the azimuthal wavenumber, m, shown in the key. The black curve represents the power spectrum of the TW itself.

is a result of a misalignment of the frequencies of TWs and convection; this lack of resonance causes the excitation to be far more sporadic or non-existent. The TW operational period is generally considerably shorter in such simulations and the convection is thus too slow to excite waves in these cases. Crucially, however, we believe that the convection driven mechanism described here is more likely to occur in the core itself. Smaller scales of convection operate in the core; unlike our overdamped simulations, these eddies will have a faster turnover time and hence higher frequencies that can match Earth's TW period. Our primary simulation allows operational frequencies—of TWs and convection—to match, enabling the excitation mechanism to be observed. The identification of a plausible mechanism to excite TWs on an intradecadal timescale in the core constitutes a major advance. It further supports the theory that TWs can exist in the core and thus also be responsible for the observed ∼6-yr variations in Earth's length-of-day.

ACKNOWLEDGEMENTS

This work was partly supported by the Natural Environment Research Council, grant NE/I012052/1. We thank two anonymous reviewers for their comments which helped to improve this paper.

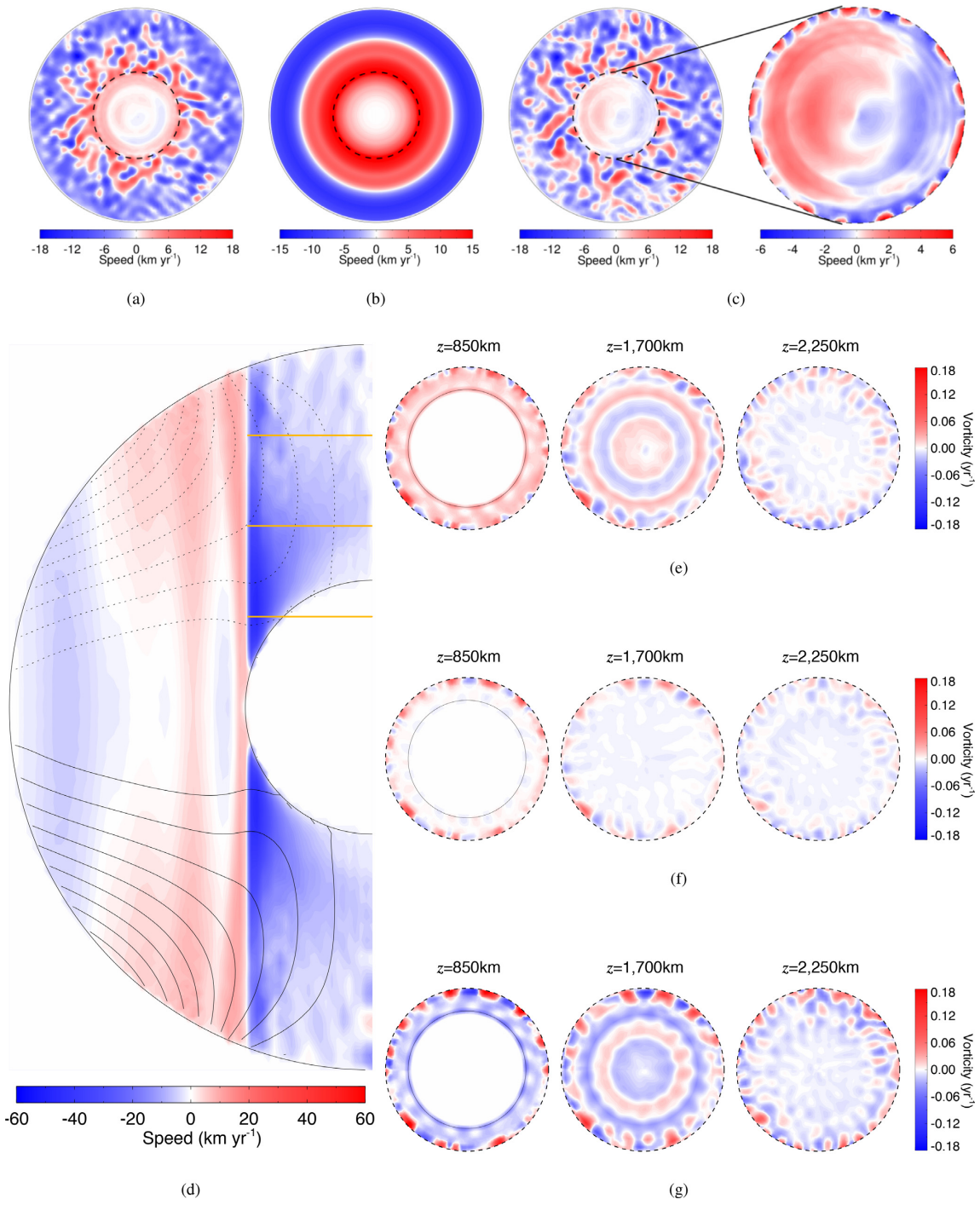

Figure 4. Convection and jets in the core. Snapshot of velocity components in $s\phi$-space at a height 1700 km above the equatorial plane at $t = 12$ yr for: (a) the total fluctuating azimuthal velocity, u'_ϕ; (b) the torsional wave speed, U_A; (c) the ageostrophic convection, $u'_{a\phi}$, with inset showing the region inside the TC. (d) Mean azimuthal velocity, $\tilde{u}_\phi$, in sz-space. Overlaid are contours of the mean radial magnetic field (solid/dotted lines indicate positive/negative field); (e–g) Vertical vorticity, ζ'_z, in $s\phi$-space at three core depths indicated in panel (d) by orange lines. Depths are shown in the figure. Only the region inside the TC is displayed, at three times: (e) 13 yr; (f) 14.5 yr; (g) 16 yr. Solid black lines indicate the location of the ICB/CMB and dashed black lines show the TC.

REFERENCES

Bloxham, J. & Gubbins, D., 1985. The secular variation of Earth's magnetic field, *Nature,* **317,** 777–781.

Bloxham, J., Zatman, S. & Dumberry, M., 2002. The origin of geomagnetic jerks, *Nature,* **420,** 65–68.

Braginsky, S.I., 1970. Torsional magnetohydrodynamic vibrations in the Earth's core and variation in day length, *Geomagn. Aeron.,* **10,** 1–8.

Buffett, B.A., Mound, J. & Jackson, A., 2009. Inversion of torsional oscillations for the structure and dynamics of Earth's core, *Geophys. J. Int.,* **177,** 878–890.

Christensen, U.R. & Wicht, J., 2015. Numerical dynamo simulations, in *Treatise of Geophysics,* 2nd edn, Vol. **8,** pp. 245–277, ed. Schubert, G., Elsevier.

Christensen, U.R. *et al.*, 2001. A numerical dynamo benchmark, *Phys. Earth planet. Inter.,* **128**(1), 25–34.

Gillet, N., Jault, D., Canet, E. & Fournier, A., 2010. Fast torsional waves and strong magnetic field within the Earth's core, *Nature,* **465,** 74–77.

Gillet, N., Jault, D. & Finlay, C.C., 2015. Planetary gyre, time-dependent eddies, torsional waves, and equatorial jets at the Earth's core surface, *J. geophys. Res.,* **120**(6), 3991–4013.

Gillet, N., Jault, D. & Canet, E., 2017. Excitation of traveling torsional normal modes in an Earth's core model, *Geophys. J. Int.,* **210**(3), 1503–1516.

Gubbins, D. & Bloxham, J., 1985. Geomagnetic field analysis—III. Magnetic fields on the core–mantle boundary, *Geophys. J. R. astr. Soc.,* **80,** 695–713.

Holme, R. & de Viron, O., 2013. Characterization and implications of intradecadal variations in length of day, *Nature,* **499**(7457), 202–204.

Jackson, A., 1997. Time dependence of geostrophic core-surface motions, *Phys. Earth planet. Inter.,* **103,** 293–311.

Jackson, A., Jonkers, A.R. & Walker, M.R., 2000. Four centuries of geomagnetic secular variation from historical records, *Phil. Trans. R. Soc. A,* **358**(1768), 957–990.

Jones, C.A., 2011. Planetary magnetic fields and fluid dynamos, *Annu. Rev. Fluid Mech.,* **43,** 583–614.

Jones, C.A., 2015. Thermal and compositional convection in the outer core, in *Treatise of Geophysics,* 2nd edn, Vol. **8,** pp. 115–159, ed. Schubert, G., Elsevier.

Jones, C.A., Boronski, P., Brun, A.S., Glatzmaier, G.A., Gastine, T., Miesch, M.S. & Wicht, J., 2011. Anelastic convection-driven dynamo benchmarks, *Icarus,* **216**(1), 120–135.

Livermore, P.W., Hollerbach, R. & Finlay, C.C., 2017. An accelerating high-latitude jet in Earth's core, *Nat. Geosci.,* **10**(1), 62–68.

McElhinny, M. & McFadden, P.L., 1998. *The Magnetic Field of the Earth: Paleomagnetism, the Core, and the Deep Mantle,* Vol. **63,** Academic Press.

Roberts, P.H. & Aurnou, J.M., 2012. On the theory of core-mantle coupling, *Geophys. astrophys. Fluid Dyn.,* **106**(2), 157–230.

Roberts, P.H. & King, E.M., 2013. On the genesis of the Earth's magnetism, *Rep. Prog. Phys.,* **76**(9), 096801.

Schaeffer, N., Jault, D., Nataf, H.-C. & Fournier, A., 2017. Turbulent geodynamo simulations: a leap towards Earth's core, *Geophys. J. Int.,* **211,** 1–29.

Sreenivasan, B. & Jones, C.A., 2006. Azimuthal winds, convection and dynamo action in the polar regions of planetary cores, *Geophys. astrophys. Fluid Dyn.,* **100**(4-5), 319–339.

Taylor, J., 1963. The magneto-hydrodynamics of a rotating fluid and the Earth's dynamo problem, *Proc. R. Soc. A,* **274,** 274–283.

Teed, R.J., Jones, C.A. & Tobias, S.M., 2014. The dynamics and excitation of torsional waves in geodynamo simulations, *Geophys. J. Int.,* **196**(2), 724–735.

Teed, R.J., Jones, C.A. & Tobias, S.M., 2015. The transition to Earth-like torsional oscillations in magnetoconvection simulations, *Earth planet. Sci. Lett.,* **419,** 22–31.

Wicht, J. & Christensen, U.R., 2010. Torsional oscillations in dynamo simulations, *Geophys. J. Int.,* **181,** 1367–1380.

Willis, A.P., Sreenivasan, B. & Gubbins, D., 2007. Thermal core–mantle interaction: exploring regimes for 'locked' dynamo action, *Phys. Earth planet. Inter.,* **165**(1), 83–92.

Zatman, S. & Bloxham, J., 1997. Torsional oscillations and the magnetic field within the Earth's core, *Nature,* **388,** 760–761.

SUPPORTING INFORMATION

Supplementary data are available at *GJI* online.

Figure S1. Thermal gradient across the TC. Time-average of (normalized) temperature in $s\phi$-space at height 1700 km above the equatorial plane.

Figure S2. Meridional sections of the azimuthal velocity, u_ϕ, averaged in ϕ at (a) $t = 9.5$ yr; (b) $t = 21$ yr.

Figure S3. Torsional wave signal and power spectrum for simulation 2. (a) Torsional wave signal. (b) Power spectrum of the ageostrophic convection, calculated at a point on the TC (at $s = r_i$, $z = r_i$) and normalized by the largest spectral mode. These plots are the same as Figs 2 and 3(b) but using data for simulation 2 (which has parameter values: $E = 5 \times 10^{-6}$, $Ra = 1.5 \times 10^8$, $Pr = 1$, $Pm = 0.2$, $B_0 = 10$).

Figure S4. Torsional wave signal and power spectrum for simulation 3. As Fig. S3, but for simulation 3 (which has parameter values: $E = 5 \times 10^{-6}$, $Ra = 1.5 \times 10^8$, $Pr = 1$, $Pm = 0.2$, $B_0 = 10$).

Figure S5. Torsional wave signal and power spectrum for simulation 4. As Fig. S3, but for simulation 4 (which has parameter values: $E = 5 \times 10^{-6}$, $Ra = 1.5 \times 10^8$, $Pr = 1$, $Pm = 0.05$, $B_0 = 10$).

Please note: Oxford University Press is not responsible for the content or functionality of any supporting materials supplied by the authors. Any queries (other than missing material) should be directed to the corresponding author for the article.